ORIGINAL ARTICLE

JBMR

# The Novel p38 Inhibitor, Pamapimod, Inhibits Osteoclastogenesis and Counteracts Estrogen-Dependent Bone Loss in Mice

Xiangde Zhao,[1,2*] Lei Ning,[1,2*] Ziang Xie,[1,2*] Zhiwei Jie,[1,2*] Xiang Li,[1,2] Xinyu Wan,[3] Xuewu Sun,[1,2] Bao Huang,[1,2] Pan Tang,[4] Shuying Shen,[1,2] An Qin,[5] Yan Ma,[1] Lu Song,[6] Shunwu Fan,[1,2] and Shuanglin Wan[1,2]

[1]Department of Orthopaedics, Sir Run Run Shaw Hospital, Zhejiang University School of Medicine, Hangzhou, China
[2]Key Laboratory of Musculoskeletal System Degeneration and Regeneration Translational Research of Zhejiang Province, Hangzhou, China
[3]First Clinical Medical College, Wenzhou Medical University, Wenzhou, China
[4]Department of Orthopedics, Huzhou Central Hospital, Zhejiang University Huzhou Hospital, Huzhou, China
[5]Department of Orthopaedics, Shanghai Key Laboratory of Orthopaedic Implant, Shanghai Ninth People's Hospital, Shanghai Jiaotong University School of Medicine, Shanghai, China
[6]Department of Oral Medicine, the Second Affiliated Hospital, Zhejiang University School of Medicine, Hangzhou, China

## ABSTRACT

Pamapimod (PAM) is a novel selective p38 mitogen-activated protein (MAP) kinase inhibitor proved to be effective in rheumatoid arthritis in phase 2 clinical trial. However, its effect on osteoclast-associated osteoporosis and the underlying mechanisms remain unclear. In this study, we showed that PAM suppressed receptor activator of nuclear factor-κB ligand (RANKL)-induced osteoclast formation via inhibition of p38 phosphorylation and subsequent c-Fos and nuclear factor of activated T cells c1 (NFATc1) expression. In addition, the downregulated NFATc1 leads to reduced expression of its targeting gene disintegrin and metalloproteinase domain-containing protein 12 (ADAM12), which was further proven to be critical for osteoclastic bone resorption. Therefore, we treated ovariectomized (OVX) mice with PAM and revealed a protective effect of PAM on osteoporosis in vivo. In conclusion, our results demonstrated PAM can prevent OVX-induced bone loss through suppression of p38/NFATc1-induced osteoclast formation and NFATc1/ADAM12-associated bone resorption. © 2018 American Society for Bone and Mineral Research.

**KEY WORDS:** OSTEOPOROSIS; OSTEOCLAST; ADAM12; P38

## Introduction

Osteoporosis is a worldwide metabolic disease affecting more than 200 million patients.[1] It is characterized by low bone mass and high susceptibility to fracture.[2] Osteoporosis increases the risk of fracture, especially fractures of the hip and spine, which not only increase the economic burden but also mortality.[3] Although many treatments targeting osteoclast have been made, further alternative treatments are required as different side effects of now available treatments exist.

Osteoclast is the only cell with the ability of bone resorption. Under the stimulation of receptor activator of nuclear factor-κB ligand (RANKL) and macrophage colony-stimulating factor (M-CSF), bone marrow macrophages can differentiate into osteoclasts.[4,5] In detail, the proliferation and survival of osteoclast precursors are guaranteed by the binding of M-CSF to its receptor, c-Fms.[6] RANKL promotes osteoclastogenesis by activating several cellular signaling pathways, including mitogen-activated protein (MAP) kinases, activator protein-1 (AP-1), and NF-κB, through its receptor RANK.[7] Then key downstream regulators like c-Fos[8,9] and NFATc1[10,11] are upregulated and activated, which further regulate the expression of osteoclast-specific genes, resulting in the formation of mature osteoclasts. Mature osteoclasts attach to the bone matrix and exert resorption activity within the sealing zone, which critically depends on the existence of F-actin.[12] Active osteoclasts secrete protons and many proteases like cathepsin K into the sealing zone to resorb bone matrix.[13]

P38 is one vital component of MAPK family and has long been reported to be involved in cell differentiation, proliferation, transcription regulation, and inflammatory responses. It has also been demonstrated that p38 regulates the expression of c-Fos and NFATc1 during osteoclast differentiation.[14,15] However, it is still interesting whether p38 inhibitors, particularly selective

Received in original form May 12, 2018; revised form November 21, 2018; accepted December 4, 2018. Accepted manuscript online December 15, 2018.
Address correspondence to: Shuanglin Wan, PhD, and Shunwu Fan, PhD, Department of Orthopaedics, Sir Run Run Shaw Hospital, Zhejiang University School of Medicine, 3 East Qingchun Road, Hangzhou, 310000, China. E-mail: wanshuanglin@zju.edu.cn (SW), shunwu_fan@zju.edu.cn (SF)
*XZ, LN, ZX, and ZJ contributed equally to this work.
Additional Supporting Information may be found in the online version of this article.
Journal of Bone and Mineral Research, Vol. 34, No. xx, Month 2019, pp 1–12
DOI: 10.1002/jbmr.3655

inhibitors, can be used for the treatment of osteolytic diseases such as osteoporosis. Indeed, a selective p38 inhibitor, pamapimod (PAM),[16] was previously used for the treatment of rheumatoid arthritis.[17] It was proven to be effective for the prevention of joint destruction with the underlying mechanisms needing further clarification.[18] Thus, this study aims to answer whether this compound could prevent osteoclast-associated osteoporosis in vivo.

ADAM12, also named meltrin-α, has been reported to be involved in fertilization,[19] muscle development,[20] and cardiac hypertrophy.[21] Recent studies demonstrate ADAM12 is involved in invasion and metastasis of tumor.[22,23] Kumasawa and colleagues reported that p38 could regulate the expression of ADAM12 in human airway smooth muscle cells.[24] ADAM12 is upregulated during the formation of osteoclast,[25–27] but the function of ADAM12 in osteoclast and the exact mechanism are still unknown. Therefore, the second aim of this study is to investigate whether this p38 inhibitor is involved in modulating osteoclast bone resorption by affecting ADAM12.

## Materials and Methods

### Reagents

The alpha modification of Eagle's medium (α-MEM), penicillin/streptomycin, and fetal bovine serum (FBS) were purchased from Gibco-BRL (Gaithersburg, MD, USA). The cell counting kit (CCK-8) was obtained from Dojindo Molecular Technology (Kumamoto, Japan). Recombinant mouse M-CSF and mouse RANKL were obtained from R&D (Minneapolis, MN, USA), and PAM was purchased from Selleck Chemicals (Shanghai, China). Specific antibodies against ERK, JNK, p38, phospho-ERK (Tr202/Tyr204), phospho-JNK (Tr183/Tyr185), phospho-p38 (Tr180/Tyr182), c-Fos, NFATc1, and α-tubulin were obtained from Cell Signaling Technology (Danvers, MA, USA). Antibody against ADAM12 was purchased from Abcam (Cambridge, MA, USA). The TRAP staining kit, and all other reagents, were purchased from Sigma-Aldrich (St. Louis, MO, USA) unless otherwise stated.

### Mouse bone marrow–derived macrophage (BMM) preparation and osteoclast differentiation

Primary BMMs were isolated from the whole bone marrow of female 6-week-old C57BL/6 mice. Briefly, cells were isolated from the femoral and tibial bone marrow and cultured in α-MEM supplemented with 10% FBS, 1% penicillin/streptomycin, and 30 ng/mL$^{-1}$ M-CSF in a 37°C, 5% $CO_2$ incubator until 90% confluence reached. The BMMs were then seeded into a 96-well plate at a density of $8 \times 10^3$ cells per well, in triplicate, in the presence of 30 ng/mL$^{-1}$ M-CSF, 50 ng/mL$^{-1}$ RANKL, and different concentrations of PAM (0, 16, 32, and 64 nM). The culture medium was replaced every 2 days until mature osteoclasts were formed. Then the cells were washed with phosphate-buffered saline (PBS) 2 times, fixed with 4% paraformaldehyde for 20 minutes, and stained for TRAP.

### Cytotoxicity assay

The cytotoxic effects of PAM on BMMs were determined using CCK-8 assay. BMMs were plated in 96-well plates at a density of $2 \times 10^4$ cells/well$^{-1}$ in triplicate in the presence of 30 ng/mL$^{-1}$ M-CSF for 24 hours. Cells were then treated with different concentrations of PAM (0, 0.02, 0.04, 0.08, 0.16, 0.31, 0.63, 1.25, 2.5 and 5 μM) plus 30 ng/mL$^{-1}$ M-CSF for 48 or 96 hours. Then, 10 μL of CCK-8 buffer was added to each well, and plates were incubated for an additional 2 hours. The optical density (OD) was then measured at a wavelength of 450 nm (650 nm reference) on an ELX800 absorbance microplate reader (Bio-Tek Instruments, Winooski, VT, USA).

### Resorption pit assay

BMMs were seeded at a density of $8 \times 10^3$ cells/well onto bovine bone slices in a 96-well plate with three replicates in the presence of 30 ng/mL$^{-1}$ M-CSF. After 24 hours, cells were treated with 50 ng/mL$^{-1}$ RANKL, 30 ng/mL$^{-1}$ M-CSF, and 0, 16, 32, or 64 nM PAM until mature osteoclasts formed. Cells were then fixed with 2.5% glutaraldehyde. Resorption pits were visualized under a scanning electron microscope (FEI Instruments, Hillsboro, OR, USA), and the bone resorption area was quantified using Image J software (National Institutes of Health, Bethesda, MD, USA). The depth of resorption pits were measured by confocal microscopy (LSM 710, Carl Zeiss, Jena, Germany) after FITC staining.

### Differentiation of osteoblastic stromal cells

Mouse mesenchymal stem cells MC3T3-E1 were cultured in α-MEM containing PAM as indicated, 50 μg/mL$^{-1}$ ascorbic acid (Sigma-Aldrich) and 10 mM β-glycerophosphate (Sigma-Aldrich) for 7 days or 21 days. The medium was changed every other day. Then cells were stained with BCIP/NBT kit (CWBIO, Beijing, China) to detect ALP and 2% Alizarin red S solution (pH 4.1) (Sigma-Aldrich) to visualize calcium deposition in the extracellular matrix. Mineralization was quantitatively assessed by measuring the absorbance of the extracted stain at 562 nm using a microplate reader after destained with ethylpyridinium chloride (Wako Pure Chemical Industries Ltd, Osaka, Japan).

### RNA extraction and quantitative real time-PCR assay

BMMs were seeded in 6-well plates at a density of $10 \times 10^4$ cells/well$^{-1}$ and cultured in α-MEM supplemented with 30 ng/mL$^{-1}$ M-CSF, 50 ng/mL$^{-1}$ RANKL, and 64 nM PAM for 0, 2, 4, or 6 days. Total RNA was extracted using the RNeasy Mini Kit (Qiagen, Valencia, CA, USA). Complementary DNA (cDNA) was synthesized using 1 μg of RNA from each sample, 2 μL of 5× PrimeScript RT Master Mix (Takara Bio, Otsu, Japan), and 4 μL of RNase free distilled water in a total volume of 10 μL. RT-PCR was performed using an ABI Prism 7500 system (Applied Biosystems, Foster City, CA, USA) with SYBR Green QPCR Master Mix (Takara Bio). The total volume (10 μL) of each PCR reaction consisted of 5 μL SYBR Green QPCR Master Mix, 3 μL ddH2O, 1 μL cDNA, and 10 μM each of forward and reverse primers. The real-time PCR reaction was performed at 95°C for 10 minutes (activation), followed by 40 cycles of 95°C for 10 seconds, 60°C for 20 seconds, and 72°C for 20 seconds (amplification), and a final extension at 72°C for 1 minute. The quantity of each target was normalized to GAPDH.

### Western blotting

BMMs were seeded in 6-well plates at a density of $5 \times 10^5$ cells · well$^{-1}$. The cells were pretreated with or without 64 nM PAM for 2 hours. Cells were then stimulated with 50 ng/mL$^{-1}$ RANKL for 0, 30, or 60 minutes. To determine the effect of PAM on NFATc1, BMMs were treated with 50 ng/mL$^{-1}$ RANKL plus 30 ng/mL$^{-1}$ M-CSF, with or without 64 nM PAM, for 0, 1, 3, or 5 days. Total protein was extracted from cultured cells using radioimmunoprecipitation assay (RIPA) lysis buffer (Sigma-

Aldrich). Lysates were centrifuged at 12,000*g* for 15 minutes, and the supernatants were collected. Proteins were resolved on 10% SDS-PAGE gels and transferred to PVDF membranes (Bio-Rad, Hercules, CA, USA). The membranes were blocked in 5% nonfat dry milk in TBST (50 mM Tris (pH 7.6), 150 mM NaCl, 0.1% Tween 20) at room temperature for 1 hour and then incubated with primary antibodies overnight at 4°C. Protein bands were visualized using the LAS-4000 Science Imaging System (Fujiflm, Tokyo, Japan).

### Small-interfering RNA (siRNA) transfection

Control siRNA and ADAM12 siRNA were purchased from GenePharma (Shanghai, China). SiRNA were transfected into BMMs using lipofectamine 3000 (Invitrogen, Carlsbad, CA, USA) and then BMMs were induced to the formation of osteoclast.

### ChIP assay

ChIP was performed by using the SimpleChIP Enzymatic Chromation IP Kit (Agarose Beads) (CST, Cambridge, MA, USA) according to the manufacturer's instructions. Precipitated DNAs from treated RAW264.7 cells were identified by PCR using specific primers that detect the binding of NFATc1 to mouse Adam12 gene.

### OVX-induced bone loss model

All animal experiments were performed in accordance with the principles and procedures of the National Institutes of Health (NIH) Guide for the Care and Use of Laboratory Animals and the guidelines for the animal treatment of Sir Run Run Shaw Hospital (Zhejiang University affiliated, Hangzhou, Zhejiang). Briefly, twenty 12-week-old C57BL/6 female mice were generally anesthetized and subjected to either a sham operation or bilateral ovariectomy (OVX). We randomly divided the mice into four groups: sham (sham operation and injection with PBS), vehicle (OVX and injection with PBS), low-dose PAM (OVX and injection with 1 $mg/kg^{-1}$ PAM), and high-dose PAM (OVX and injection with 2 $mg/kg^{-1}$ PAM). The mice were injected intraperitoneally with PAM every other day for 6 weeks. All mice were euthanized at the end of 6 weeks. Uteri were isolated and weighed to confirm the effects of OVX. Left tibia from each mouse was fixed in 4% paraformaldehyde for micro-CT and histological studies. Right tibia and femur from each mouse was frozen in liquid nitrogen after dissection for the subsequent RNA extraction and quantitative PCR. To investigate PAM's therapeutic effect on osteoporosis, 20 twelve-week-old C57BL/6 female mice were generally anesthetized and subjected to either a sham operation or bilateral ovariectomy (OVX). We randomly divided the mice into four groups: sham (sham operation and injection with PBS), vehicle (OVX and injection with PBS), low-dose PAM (OVX and injection with 1 $mg/kg^{-1}$ PAM), and high-dose PAM (OVX and injection with 2 $mg/kg^{-1}$ PAM). Eight weeks after OVX, the mice were injected intraperitoneally with PAM every other day for 6 weeks. All mice were injected with calcein (12.5 mg/kg; Sigma) 10 days and 3 days before death. Tibias were fixed in 4% paraformaldehyde for micro-CT and histological studies. Tibias of another side were fixed for undecalcificated bone slicing.

### Micro-CT scanning

The fixed tibias were analyzed using a high-resolution micro-CT scanner (SkyScan 1072; Bruker microCT, Kontich, Belgium). The scanning protocol was set at an isometric resolution at 9 μm and X-ray energy settings of 80 kV and 80 μA. Bone volume per tissue volume (BV/TV), bone surface to bone volume (BS/BV), trabecular thickness (Tb.Th), number (Tb.N), and separation (Tb.Sp), and porosity were measured using the resident reconstruction program (SkyScan). The fixed tibias were decalcified in 10% EDTA for 3 weeks and then embedded in paraffin.

### Histological analysis

The specimens were examined and photographed under a high-quality microscope. The number of osteoblast and TRAP-positive multinucleated osteoclasts per field (Oc.S/BS) and eroded surface (ES/BS) were examined in each sample.

### Statistical analysis

The data were expressed as means ± SEM (standard error of the mean). The results were analyzed using Prism 7 (GraphPad Software Inc, San Diego, CA, USA) for Windows. The Student's *t* test was used to make comparisons between two groups. $p < 0.05$ indicated a significant difference between groups.

## Results

### Pamapimod suppressed RANKL-induced osteoclastogenesis in vitro

We first examined the cytotoxicity effect of PAM on primary BMMs for 48 and 96 hours. As shown in Fig. 1*B*, no cytotoxicity was found at the dose of 5 μM. To explore whether PAM can affect RANKL-induced osteoclastogenesis in vitro, we treated BMMs with M-CSF, RANKL, and PAM at the dose of 16 nM, 32 nM, and 64 nM. Apparent suppression of PAM on the formation of mature osteoclasts could be found at the dose of 32 nM and only several mature osteoclasts could be found when treated at 128 nM (Fig. 1*C*). The number of mature osteoclasts and area of osteoclasts decreased in a concentration-dependent manner. The size of mature osteoclast and the number of mature osteoclast nuclei reduced dramatically in the 64 nM group compared with the control group (Fig. 1*D*). To make a better understanding of the suppressive role of PAM during the differentiation of osteoclast, 64 nM PAM was added to osteoclast inductive medium at different time points during osteoclast formation. As shown in Fig. 1*E*, osteoclastic formation was dramatically repressed as PAM was added at an early stage of osteoclast differentiation (day 1–3). When PAM was added at the middle stage of osteoclast differentiation (day 3–5), fewer areas of osteoclasts and number of osteoclasts with 10 or more nuclei could be found compared with control. However, there was no difference in the number of mature osteoclasts between the day 3–5 group and the control group. Smaller mature osteoclasts could be found when PAM was added at a late stage of osteoclast differentiation (day 5–7) with a reduced number of osteoclast with 5 to 10 nuclei compared with control (Fig. 1*E*, *F*). Therefore, PAM mainly exhibits its suppressive role on osteoclast formation at the early stage of osteoclast differentiation.

### Expression of osteoclast-related genes were suppressed by pamapimod in vitro

To make a better understanding of the inhibitory effect of PAM on osteoclasts, we measured the mRNA expression of osteoclast-related genes such as DC-STAMP, CTSK, c-Fos, NFATc1, ATP6v0d2, and TRAP. Osteoclast-related gene expression was

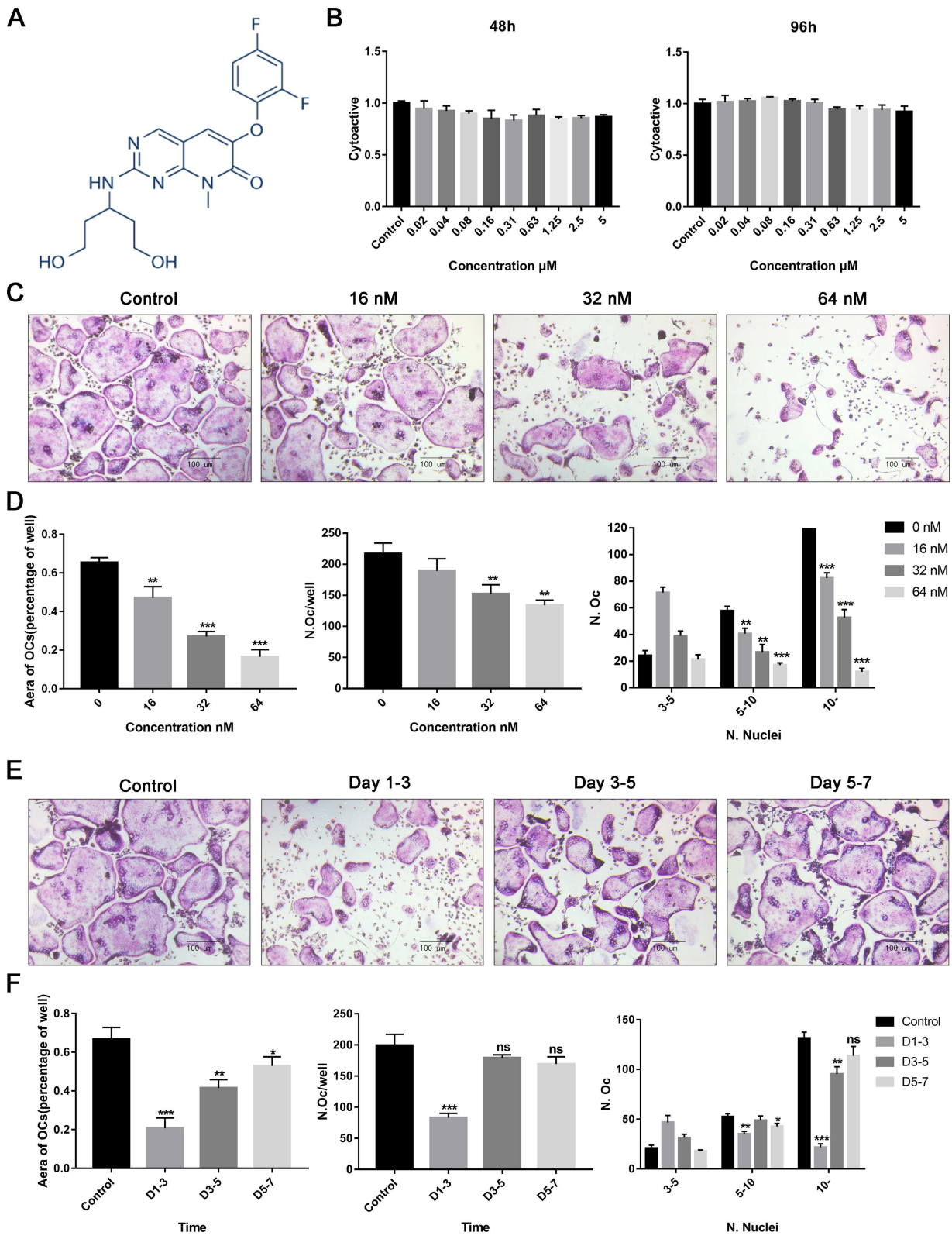


**Fig. 1.** Pamapimod inhibited RANKL-induced osteoclastogenesis without cytotoxic effects in vitro. (*A*) The structure of pamapimod. (*B*) Cytoactive of PAM-treated BMMs tested by CCK-8 assays at 48 and 96 hours. (*C*) BMMs were treated with various concentrations of PAM, M-CSF (30 ng/mL$^{-1}$), and RANKL (50 ng/mL$^{-1}$) for 5 days. Then the cells were fixed with 4% paraformaldehyde and stained for TRAP. (*D*, *F*) The number and areas of TRAP$^{+}$ multinuclear cells were determined as described in Materials and Methods ($^{*}p < 0.05$; $^{**}p < 0.01$; $^{***}p < 0.001$). (*E*) TRAP$^{+}$ BMMs after the treatment with 0.64 nM PAM for the indicated days during osteoclastogenesis. Data are expressed as means ± SEM, $n = 5$–7.

suppressed conspicuously after PAM was added compared with the upregulation of them in the control (Fig. 2). PAM showed no suppression on the formation of osteoblast as the expression of alkaline phosphatase (ALP), Osteocalcin (OCN), and Runt-related transcription factor 2 (RUNX2) did not show obvious change after the treatment of PAM under the concentration of 800 nM (Supplemental Fig. S1*A*, *B*, *D*, *F*). The differentiation and mineralization of osteoblast was not affected as well (Supplemental Fig. S1*C*, *E*).

## Pamapimod attenuated bone resorption capacity of mature osteoclasts partially by downregulation of ADAM12

To further evaluate the role of PAM on the osteoclastic bone resorption capacity, we added PAM to the medium after BMMs were plated on the bovine bone slices in 96-well plates. Bone resorption area was decreased obviously as PAM was added, especially at the concentration of 64 nM (Fig. 3*A*). Immunofluorescence assay was performed because actin ring had been regarded as an essential part during osteoclastic bone resorption. The formation of actin belt also decreased significantly in the presence of 64 nM PAM compared with the control group (Fig. 3*B*, *C*).

As mentioned in the introduction, ADAM12 was reported to be regulated by p38 and had been implicated in a variety of biological processes involving cell-cell and cell-matrix interactions, including fertilization, muscle development, and osteoclast formation, so we examined the expression of ADAM12 during osteoclast formation. Distinctly downregulated expression could be observed during osteoclast formation with the treatment of PAM and RANKL compared with the control (Fig. 3*D*). To further elucidate the mechanism of ADAM12 on osteoclast formation, we examined the number of multinuclear $TRAP^+$ osteoclasts after knockdown of ADAM12 using siRNA against mouse ADAM12 (Fig. 3*E*). However, we found no obvious difference of $TRAP^+$ osteoclast number and area after ADAM12 knockdown (Fig. 3*F*, *G*). Intriguingly, ADAM12 accumulated in close proximity to actin belt in mature osteoclast (Fig. 3*H*). It was reasonable to predict that ADAM12 was associated with the bone resorption function of osteoclast because extensive reports argued that F-actin was involved in osteoclast function. To examine whether it can affect bone resorption capacity of osteoclasts, we silenced ADAM12 after BMMs were plated on bovine bone slices. The bone resorption depth was much shallower after knockdown of ADAM12 compared with normal control, even though no conspicuous bone resorption area difference was found (Fig. 3*I*, *J*). Taken together, PAM suppressed ADAM12 expression and thus attenuated bone resorption in vitro.

## Pamapimod inhibited p38/NFATc1 pathway to suppress osteoclast formation and blocked NFATc1/ADAM12 cascades to attenuate bone resorption

To clarify the underlying mechanisms of PAM on osteoclast formation and bone resorption, we examined MAPK signaling

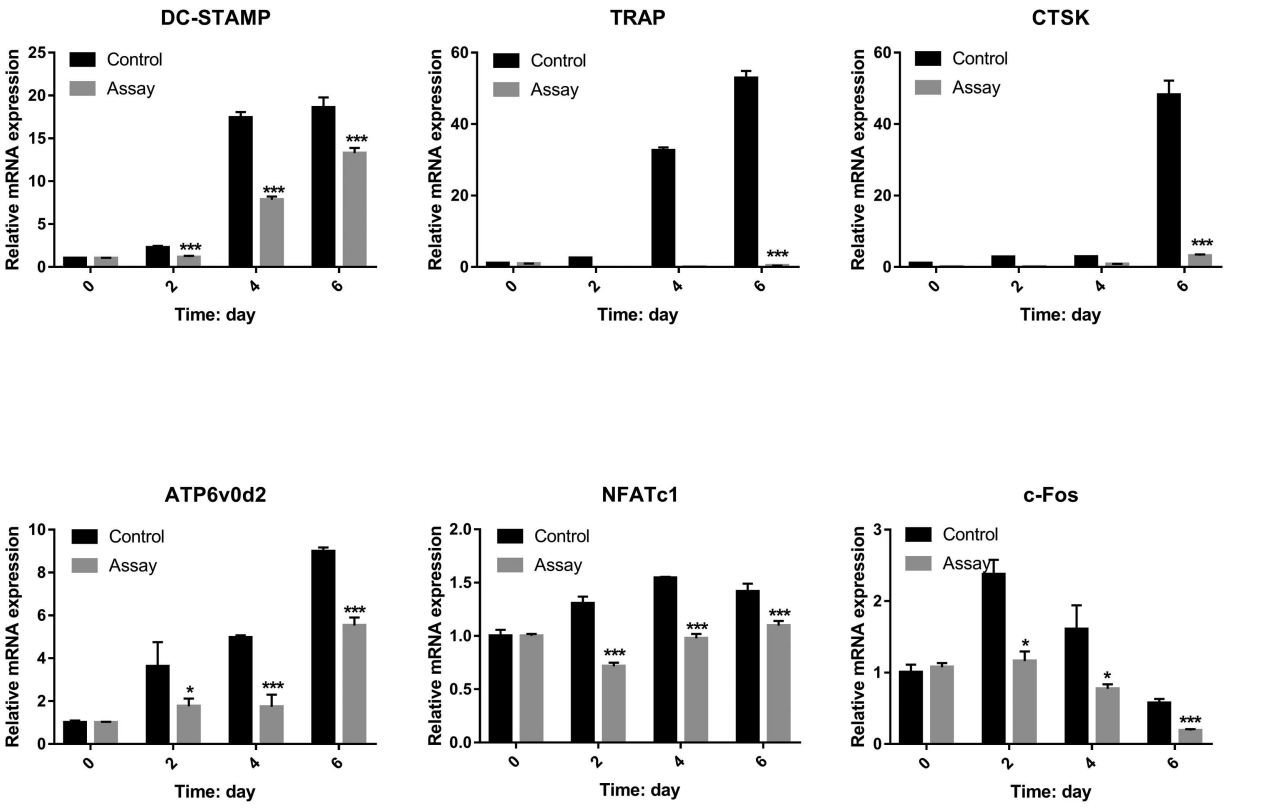


**Fig. 2.** Pamapimod inhibited RANKL-induced osteoclast-specific gene expression in vitro. Expression of the osteoclast-specific genes TRAP, CTSK, NFATc1, c-Fos, DC-STAMP, and ATP6v0d2 in BMMs treated with 64 nM PAM, M-CSF (30 ng/mL$^{-1}$), and RANKL (50 ng/mL$^{-1}$) for 0, 2, 4, or 6 days. Gene expression was analyzed by real-time PCR. mRNA expression levels were normalized relative to the expression of GAPDH ($^*p < 0.05$; $^{**}p < 0.01$; $^{***}p < 0.001$). Data are expressed as means ± SEM, $n = 5$.

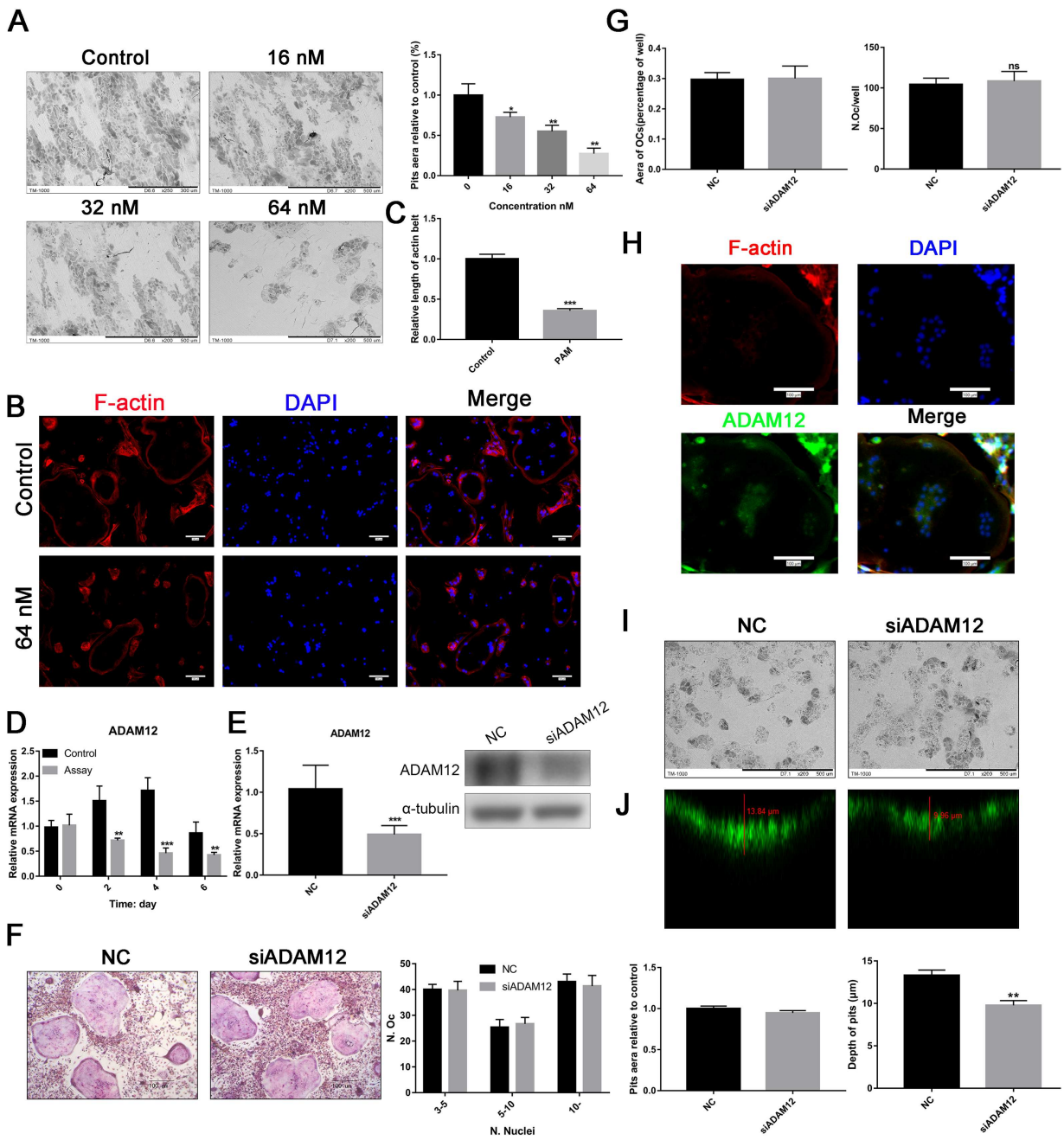


**Fig. 3.** Pamapimod inhibited osteoclastic bone resorption in vitro partially by downregulation of ADAM12. (*A*) BMMs were seeded onto bone slices and treated as described in Fig. 1*C* for 7 days. Scanning electron microscope (SEM) images of bone resorption pits are shown and resorption pit areas were measured using Image J. (*B*) Representative images for actin belt formation. (*C*) The perimeter of the actin belt was measured using Image J. (*D*) Gene expression of ADAM12 in BMMs treated with 64 nM PAM, M-CSF (30 ng/mL$^{-1}$), and RANKL (50 ng/mL$^{-1}$) for 0, 2, 4, or 6 days. (*E*) mRNA and protein level of ADAM12 in BMMs after transfection of siRNA of ADAM12. (*F*, *G*) Images and statistics of the formation of TRAP$^{+}$ osteoclasts after knockdown of ADAM12. (*H*) Immunofluorescence images of ADAM12 (green), DAPI (blue), and actin belt (red). (*I*) Images and statistics of osteoclastic bone resorption pits after knockdown of ADAM12 ($^{*}p < 0.05$; $^{**}p < 0.01$; $^{***}p < 0.001$). Data are expressed as means ± SEM, $n = 6$–7.

pathways, which mainly include c-Jun N-terminal kinase (JNK), p38, and extracellular signal-regulated kinase (ERK). BMMs were treated with RANKL, with or without PAM for 0, 30, and 60 minutes. Along with the stimulation of RANKL for 30 minutes without PAM, JNK, p38, and ERK were activated. However, the phosphorylation of p38 was sharply attenuated after PAM was added for 30 minutes compared with control. The phosphorylation of JNK and ERK were not affected (Fig. 4*A*, *B*). Then we tested the expression of two vital transcription proteins, NFATc1, which is significant for osteoclast differentiation, and c-Fos, which is directly upstream of NFATc1. Increasing expression of c-Fos and NFATc1 could be observed after stimulation of RANKL for 0 day, 1 day, 3 days, and 5 days. However, the expression of c-Fos and

NFATc1 were downregulated correspondingly as PAM was added (Fig. 4*C*, *D*).

In addition to suppression of NFATc1 by treatment with PAM, we also found the nuclear translocation of NFATc1 was inhibited by PAM (Fig. 4*E*). Interestingly, the nuclear translocation of NFATc1 is important for ADAM12 expression. Our ChIP assay revealed that ADAM12 could be directly regulated by NFATc1 (Fig. 4*F*). The expression of CTSK, TRAP, ATP6v0d2, DC-STAMP, and NFATc1 were not affected by silencing of ADAM12 (Supplemental Fig. S2). These results suggest that PAM suppresses osteoclastogenesis by suppressing p38 MAPK-NFATc1 signaling pathway and inhibits bone resorption partially by decreasing NFATc1-mediated ADAM12 expression.

## Pamapimod prevented OVX-induced bone loss in vivo

OVX-induced mouse osteoporosis model was utilized to investigate the effects of PAM treatment on osteoporosis. This

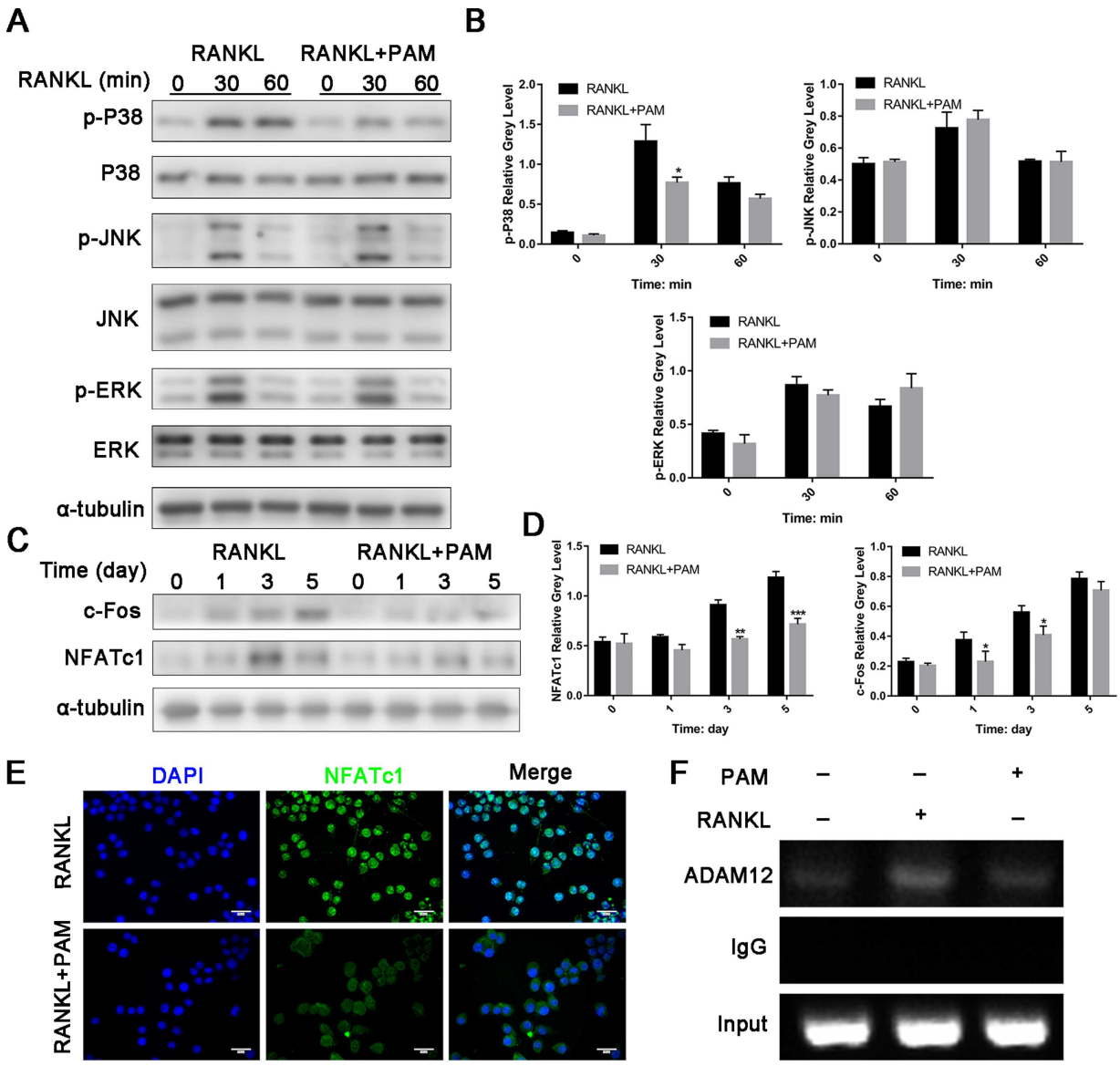


**Fig. 4.** Pamapimod inhibited osteoclastogenesis by impairing p38 MAPK and bone resorption partially by p38-NFATc1-ADAM12 in vitro. (*A*) BMMs were treated with or without 64 nM PAM for 2 hours and then treated with 50 ng/mL$^{-1}$ RANKL for the indicated periods. Cell lysates were analyzed using Western blotting. The expression of phosphorylated ERK, p38, and JNK and total ERK, p38, and JNK were assessed. (*B*) The gray levels of phosphorylated ERK, p38, and JNK were quantified and normalized to total ERK, p38, and JNK using Image J. (*C*) BMMs were treated with RANKL, with or without 64 nM PAM, for the indicated periods. Cell lysates were analyzed using Western blotting. The expression of NFATc1, c-Fos, and α-tubulin was evaluated. (*D*) The gray levels of NFATc1 and c-Fos were quantified and normalized to α-tubulin using Image J. (*E*) RAW264.7 cells were pretreated with 64 nM PAM for 2 hours, and then RANKL was added for 3 hours. Nuclei translocation of NFATc1 was analyzed using immunofluorescence. (*F*) Nuclear extracts from RANKL and PAM-treated RAW264.7 cells were used to assess whether NFATc1 could bind to the promoter region of ADAM12 using anti-NFATc1 antibody and rabbit IgG. Scale bars = 100 μm. ($^{*}p < 0.05$; $^{**}p < 0.01$; $^{***}p < 0.001$.) Data are expressed as means ± SEM, $n = 5$.

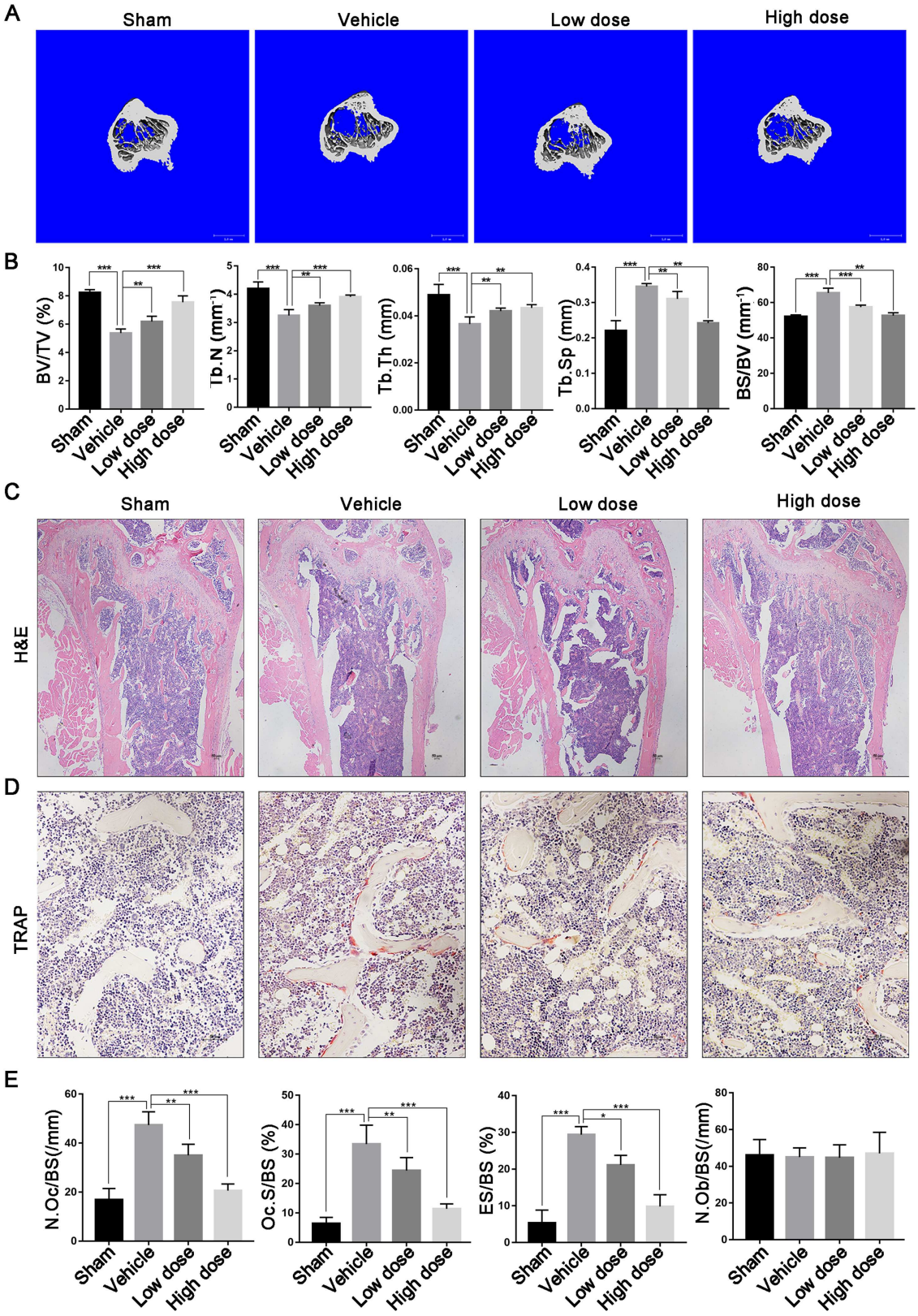


**Fig. 5.** Pamapimod effectively prevented OVX-induced bone loss in vivo. (*A*) The tibias of all mice were scanned with a high-resolution micro-CT. Scale bars = 100 μm. (*B*) Calculation of the microstructural indices was performed for the micro-CT data. Microstructural indices include bone volume/tissue volume (BV/TV), bone surface/bone volume (BS/BV), trabecular separation (Tb.Sp), trabecular thickness (Tb.T), and trabecular number (Tb.N). (*C*) Sections of tibias were stained with H&E and TRAP. Scale bars = 50 μm. (*D*) The number of osteoclasts per field of tissue (N.Oc/BS), the number of osteoblasts per field (N.Ob/BS), and eroded surface (ES/BS) in sections stained by TRAP ($^{*}p < 0.05$; $^{**}p < 0.01$; $^{***}p < 0.001$). Data are expressed as means ± SEM, $n = 5$.

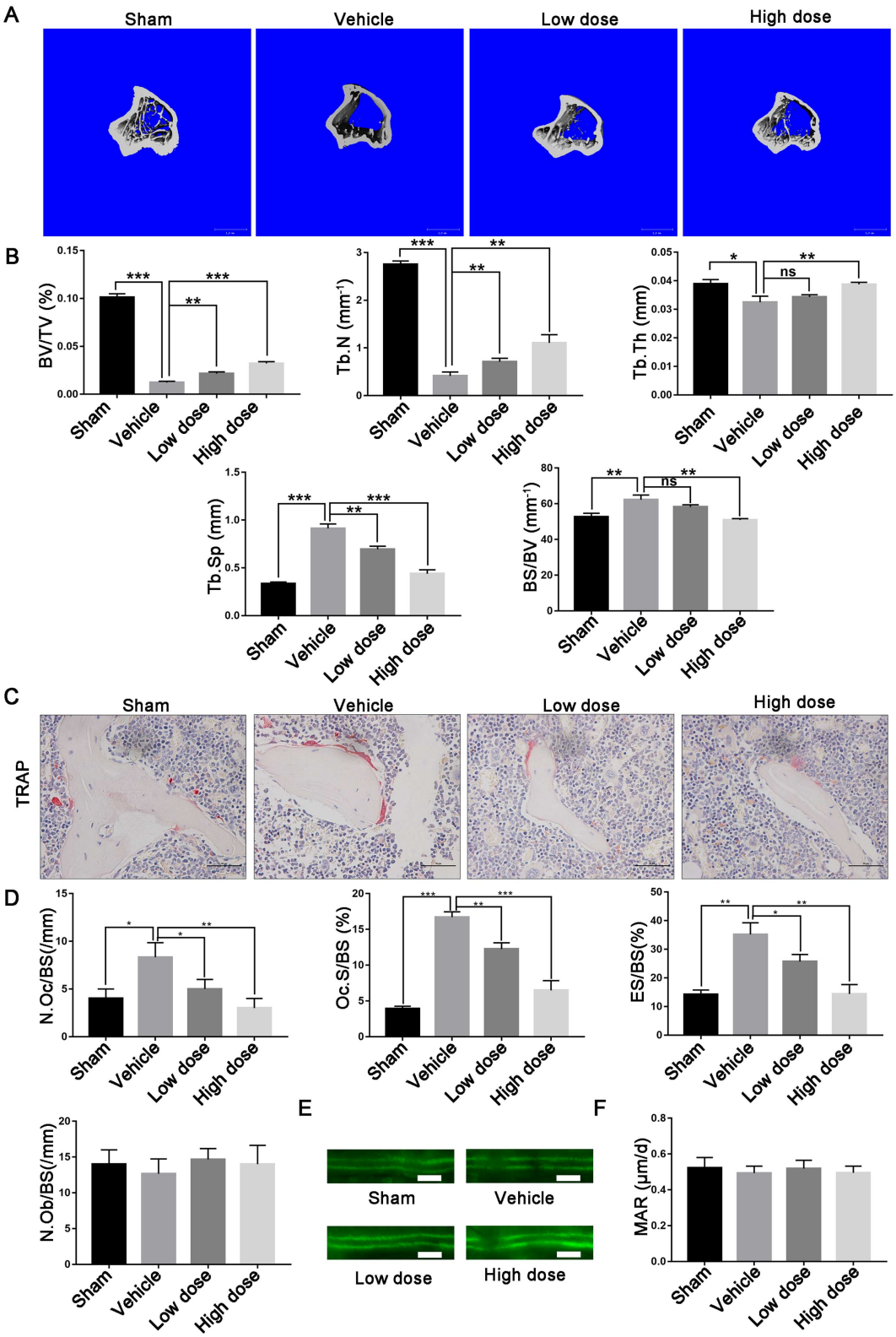


**Fig. 6.** Pamapimod showed therapeutic effect on osteoporosis in vivo. (*A*) The tibias of all mice were scanned with a high-resolution micro-CT. Scale bars = 100 μm. (*B*) Calculation of the microstructural indices was performed for the micro-CT data. Microstructural indices include bone volume/tissue volume (BV/TV), bone surface/bone volume (BS/BV), trabecular separation (Tb.Sp), trabecular thickness (Tb.T), and trabecular number (Tb.N). (*C*) Sections of tibias were stained with TRAP. Scale bars = 50 μm. (*D*) The number of osteoclasts per field of tissue (N.Oc/BS), the number of osteoblasts per field (N. Ob/BS), and eroded surface (ES/BS) in sections stained by TRAP. (*E*) Photomicrographs of fluorochrome label in each group. (*F*) Statistic of mineral apposition rate (MAR) in *E*. Scale bars = 10 μm. ($^{*}p < 0.05$; $^{**}p < 0.01$; $^{***}p < 0.001$.) Data are expressed as means ± SEM, $n = 5$.

model was established successfully as the decreased weight of uterus and increased mouse body weight shown in Supplemental Fig. S3. Mice were treated with PAM by intraperitoneal injection for 6 weeks after OVX operation, then micro-computed tomography (CT) was used to analyze the bone loss in the proximal tibia (Fig. 5*A*). Microstructural parameters such as BV/TV, Tb.Th, and Tb.N had a serious decrease and an increase of BS/BV and Tb.Sp in the vehicle-treated group compared with the sham group. Compared with the vehicle-treated group, there was an increase in the values of BV/TV, Tb.Th, and Tb.N but a decrease of BS/BV and Tb.Sp in the PAM-treated group in a dose-dependent manner (Fig. 5*A*, *B*). Hematoxylin and eosin (H&E) staining further verified the beneficial effect of PAM to the bone mass of OVX mice (Fig. 5*C*). Number of multinucleated osteoclasts was increased remarkably and the percentage of osteoclast surface per bone surface (Oc.S/BS%) and eroded surface (ES/BS) also had a sharp rise in the vehicle-treated group compared with the sham group as shown by the TRAP staining images. The protective effects of PAM could be further confirmed as both the number of multinucleated osteoclasts and Oc.S/BS% declined in the PAM-treated group compared with the vehicle-treated group (Fig. 5*C*, *D*). However, PAM had no inhibitory effect on osteogenesis as shown in Fig. 5*E*. The mRNA levels of osteoclast-related genes, ADAM12 included, were also downregulated in the PAM-treated group in a dose-dependent manner compared with the vehicle-treated group (Supplemental Fig. S4). To investigate PAM's therapeutic effect on osteoporosis, osteoporotic mice (8 weeks after OVX) were injected with PAM for 6 weeks accordingly. PAM increased the bone mass compared with the vehicle group (Fig. 6*A*, *B*) and decreased $TRAP^+$ cell number (Fig. 6*C*, *D*). Consistent with the previous results, PAM also had no inhibitory effect on osteogenesis as shown in Fig. 6*E*, *F*.

## Discussion

Although many treatments targeting osteoclasts have been made, further alternative treatments are required because different side effects of now available treatments exist. Long-term hormone-replacement therapy could increase the risk of vaginal bleeding, deep vein thrombosis, pulmonary embolism,[28] breast tenderness, and even breast cancer.[29,30] A side effect of bisphosphonates, a rare but serious osteonecrosis of the jaw, has also been reported.[31,32] Multinucleated osteoclasts, formed by the fusion of monocyte/macrophage family, are the only cells capable of bone resorption. Excessive osteoclast activity results in bone-related disease, including postmenopausal osteoporosis, rheumatoid arthritis (RA), and Paget's disease.[33,34] Here, we showed PAM, a novel selective p38 MAPK inhibitor,[16] inhibits the formation and resorption of multinucleated osteoclasts.

p38 MAPK have four isoforms, including MAPK14, MAPK11, MAPK12, and MAPK13.[35,36] Among the four isoforms, MAPK14 and MAPK 11 play a significant role in osteoclast differentiation.[37,38] There are a large number of reports that demonstrate that p38 regulates the expression of c-Fos, an upstream of NFATc1, or NFATc1 through a different way, such as MITF,[39] ATF3,[40] CREB,[41] and MSK1.[42] So selective inhibitors targeting MAPK14 and MAPK11 are potential new treatments for osteoclast-associated osteoporosis. PAM, a selective p38 MAPK inhibitor targeting MAPK14 and MAPK11,[16] has been previously showed to inhibit the progression of RA.[16,18] However, the role of PAM on osteoporosis has not been reported.

In this study, we demonstrated PAM could inhibit the formation of osteoclast in vitro through blocking of the p38 MAPK signaling pathway. The underlying mechanism is in agreement with previous studies. The inhibition of p38 phosphorylation suppressed the expression of its downstream protein c-Fos. Moreover, it subsequently decreased the expression of key transcriptional factor NFATc1. Although PAM showed dramatic inhibition of osteoclastogenesis in a dose-dependent manner, the inhibitory effect was only shown obviously when PAM was added at an early stage (day 1–3). This result is consistent with the previous reports that p38 MAPK phosphorylated in BMMs at the stimulation of RANKL but not in mature osteoclasts. Thus, our study for the first time showed that PAM is an effective compound for the treatment of osteoporosis by inhibiting osteoclast formation. More importantly, we also demonstrate that ADAM12 is involved in bone resorption capacity without affection of osteoclast fusion. ADAM12 is regulated by NFATc1. Therefore, suppression of NFATc1 by PAM not only inhibits osteoclast formation but also attenuates bone resorption capacity partially by downregulation of ADAM12. Here, we first found that ADAM12 is regulated by NFATc1 because chromatin immunoprecipitation (ChIP) results showed that NFATc1 binds to the promoter region of ADAM12 and increases the transcription of ADAM12 after stimulation of RANKL. Reports show that ADAM12 is upregulated upon osteoclast formation and could be involved in osteoclast formation.[25–27] However, the exact function and mechanism of ADAM12 in osteoclasts have not been elaborated yet. Indeed, our results demonstrated that during osteoclast differentiation, BMMs treated with ADAM12 siRNA showed normal osteoclastogenesis, which is different from Abe and colleagues' result.[25] This may due to different methods being used, as Abe and colleagues used antisense oligonucleotide transfection of ADAM12 gene in alveolar macrophages of 8-week-old male Swiss Webster mice. Further immunofluorescence results led us to the idea that ADAM12 is involved in osteoclastic bone resorption capacity as ADAM12 accumulated in close proximity to actin belt in mature osteoclasts. Bone resorption pit assay indicated that the knockdown of ADAM12 affects osteoclastic bone resorption capacity. Meanwhile, PAM showed no repression on the formation of osteoblast and osteoblastic bone formation in vitro and in vivo. Because of its dual roles on osteoclast formation and osteoclast resorption, we proved that PAM exerted a protective role in OVX-induced bone loss in vivo. Taken together, our study suggests that PAM can be used potentially as a novel drug for the treatment of osteoporosis.

However, there are certain weaknesses existing in our study. For instance, the underlying mechanism of ADAM12 on bone resorption may lead to better understanding of its role in osteoclasts.

In conclusion, our results showed that PAM inhibits osteoclast differentiation and function both in vitro and in vivo. Our study also demonstrated that ADAM12, regulated by p38/NFATc1 axis, is involved in bone resorption. Thus, our results manifest that PAM could be a potential treatment for osteoporosis and ADAM12 may be a new target for osteoporosis treatment.

## Disclosures

All authors state that they have no conflicts of interest.

## Acknowledgments

This study was sponsored by Medical and Health Science and Technology Planning Project of Zhejiang Province (2017KY082, 2018KY493), Natural Science Foundation of Zhejiang Province (LY18H060001, LQ18H250001, LY16H060004), Key Project of Zhejiang Provincial Natural Science Foundation (LZ15H06002), Key Project of Zhejiang Medical Science and Technology Plan (2016145597) and National Natural Science Foundation of China (81871797, 81601925). No benefits in any form have been or will be received from a commercial party related directly or indirectly to the subject of this study.

Authors' roles: SW, ZX, and AQ designed the study. XZ, LN, ZJ, XW, and ZX carried out experiments. ZX, XL, XS, BH, and PT analyzed data. AQ, SW, and SF interpreted results of experiments. SS, YM and LS prepared the figures. XZ, LN, and ZX wrote the manuscript. All authors reviewed the manuscript.

## References

1. Strom O, Borgstrom F, Kanis JA, et al. Osteoporosis: burden, health care provision and opportunities in the EU: a report prepared in collaboration with the International Osteoporosis Foundation (IOF) and the European Federation of Pharmaceutical Industry Associations (EFPIA). Arch Osteoporos. 2011;6:59–155.
2. Johnell O, Kanis JA, Oden A, et al. Predictive value of BMD for hip and other fractures. J Bone Miner Res. 2005;20(7):1185–94.
3. Center JR, Nguyen TV, Schneider D, Sambrook PN, Eisman JA. Mortality after all major types of osteoporotic fracture in men and women: an observational study. Lancet (London, England). 1999; 353(9156):878–82.
4. Lagasse E, Weissman IL. Enforced expression of Bcl-2 in monocytes rescues macrophages and partially reverses osteopetrosis in op/op mice. Cell. 1997;89(7):1021–31.
5. Kong YY, Yoshida H, Sarosi I, et al. OPGL is a key regulator of osteoclastogenesis, lymphocyte development and lymph-node organogenesis. Nature. 1999;397(6717):315–23.
6. Gingery A, Bradley E, Shaw A, Oursler MJ. Phosphatidylinositol 3-kinase coordinately activates the MEK/ERK and AKT/NFkappaB pathways to maintain osteoclast survival. J Cell Biochem. 2003; 89(1):165–79.
7. Li C, Yang Z, Li Z, et al. Maslinic acid suppresses osteoclastogenesis and prevents ovariectomy-induced bone loss by regulating RANKL-mediated NF-kappaB and MAPK signaling pathways. J Bone Miner Res. 2011;26(3):644–56.
8. Monje P, Hernandez-Losa J, Lyons RJ, Castellone MD, Gutkind JS. Regulation of the transcriptional activity of c-Fos by ERK. A novel role for the prolyl isomerase PIN1. J Biol Chem. 2005;280(42):35081–4.
9. Tanos T, Marinissen MJ, Leskow FC, et al. Phosphorylation of c-Fos by members of the p38 MAPK family. Role in the AP-1 response to UV light. J Biol Chem. 2005;280(19):18842–52.
10. Takayanagi H, Kim S, Koga T, et al. Induction and activation of the transcription factor NFATc1 (NFAT2) integrate RANKL signaling in terminal differentiation of osteoclasts. Dev Cell. 2002;3(6):889–901.
11. Matsuo K, Galson DL, Zhao C, et al. Nuclear factor of activated T-cells (NFAT) rescues osteoclastogenesis in precursors lacking c-Fos. J Biol Chem. 2004;279(25):26475–80.
12. Vaananen HK, Zhao H, Mulari M, Halleen JM. The cell biology of osteoclast function. J Cell Sci. 2000;113(Pt 3):377–81.
13. Teti A, Marchisio PC, Zallone AZ. Clear zone in osteoclast function: role of podosomes in regulation of bone-resorbing activity. Am J Physiol. 1991;261(1 Pt 1):C1–7.
14. Sharma SM, Bronisz A, Hu R, et al. MITF and PU.1 recruit p38 MAPK and NFATc1 to target genes during osteoclast differentiation. J Biol Chem. 2007;282(21):15921–9.
15. Huang H, Chang EJ, Ryu J, Lee ZH, Lee Y, Kim HH. Induction of c-Fos and NFATc1 during RANKL-stimulated osteoclast differentiation is mediated by the p38 signaling pathway. Biochem Biophys Res Commun. 2006;351(1):99–105.
16. Goldstein DM, Soth M, Gabriel T, et al. Discovery of 6-(2,4-difluorophenoxy)-2-[3-hydroxy-1-(2-hydroxyethyl)propylamino ]-8-methyl-8H-p yrido[2,3-d]pyrimidin-7-one (pamapimod) and 6-(2,4-difluorophenoxy)-8-methyl-2-(tetrahydro-2H-pyran-4-ylamino)pyrido[2,3-d]py rimidin-7(8H)-one (R1487) as orally bioavailable and highly selective inhibitors of p38alpha mitogen-activated protein kinase. J Med Chem. 2011;54(7): 2255–65.
17. Cohen SB, Cheng TT, Chindalore V, et al. Evaluation of the efficacy and safety of pamapimod, a p38 MAP kinase inhibitor, in a double-blind, methotrexate-controlled study of patients with active rheumatoid arthritis. Arthritis Rheum. 2009;60(2):335–44.
18. Hill RJ, Dabbagh K, Phippard D, et al. Pamapimod, a novel p38 mitogen-activated protein kinase inhibitor: preclinical analysis of efficacy and selectivity. J Pharmacol Exp Ther. 2008;327(3):610–9.
19. Sahraravand M, Laitinen P, Jarvela I, Ryynanen M. First-trimester maternal serum ADAM12-s and PAPP-A levels are altered in pregnancies conceived after assisted reproduction techniques (ART). Prenat Diagn. 2016;36(2):163–9.
20. Yagami-Hiromasa T, Sato T, Kurisaki T, Kamijo K, Nabeshima Y, Fujisawa-Sehara A. A metalloprotease-disintegrin participating in myoblast fusion. Nature. 1995;377(6550):652–6.
21. Asakura M, Kitakaze M, Takashima S, et al. Cardiac hypertrophy is inhibited by antagonism of ADAM12 processing of HB-EGF: metalloproteinase inhibitors as a new therapy. Nat Med. 2002; 8(1):35–40.
22. Wang J, Voellger B, Benzel J, et al. Metalloproteinases ADAM12 and MMP-14 are associated with cavernous sinus invasion in pituitary adenomas. Int J Cancer. 2016;139(6):1327–39.
23. Luo ML, Zhou Z, Sun L, et al. An ADAM12 and FAK positive feedback loop amplifies the interaction signal of tumor cells with extracellular matrix to promote esophageal cancer metastasis. Cancer Lett. 2018; 422:118–28.
24. Kumasawa F, Hashimoto S, Mizumura K, et al. Mitogen-activated protein kinase (MAPK) regulates leukotriene D4-induced HB-EGF and ADAM12 expression in human airway smooth muscle cells. Asian Pac J Allergy Immunol. 2013;31(1):58–66.
25. Abe E, Mocharla H, Yamate T, Taguchi Y, Manolagas SC. Meltrin-alpha, a fusion protein involved in multinucleated giant cell and osteoclast formation. Calcif Tissue Int. 1999;64(6):508–15.
26. Ma G, Ainola M, Liljestrom M, et al. Increased expression and processing of ADAM 12 (meltrin-alpha) in osteolysis associated with aseptic loosening of total hip replacement implants. J Rheumatol. 2005;32(10):1943–50.
27. Verrier S, Hogan A, McKie N, Horton M. ADAM gene expression and regulation during human osteoclast formation. Bone. 2004;35(1): 34–46.
28. Grodstein F, Stampfer MJ, Goldhaber SZ, et al. Prospective study of exogenous hormones and risk of pulmonary embolism in women. Lancet (London, England). 1996;348(9033):983–7.
29. Bergkvist L, Persson I. Hormone replacement therapy and breast cancer. A review of current knowledge. Drug Saf. 1996;15(5): 360–70.
30. Colditz GA, Hankinson SE, Hunter DJ, et al. The use of estrogens and progestins and the risk of breast cancer in postmenopausal women. N Engl J Med. 1995;332(24):1589–93.
31. Bamias A, Kastritis E, Bamia C, et al. Osteonecrosis of the jaw in cancer after treatment with bisphosphonates: incidence and risk factors. J Clin Oncol. 2005;23(34):8580–7.
32. Delmas PD, Bjarnason NH, Mitlak BH, et al. Effects of raloxifene on bone mineral density, serum cholesterol concentrations, and uterine endometrium in postmenopausal women. N Engl J Med. 1997; 337(23):1641–7.
33. Sambrook P, Cooper C. Osteoporosis. Lancet. 2006;367(9527): 2010–8.
34. Walsh MC, Kim N, Kadono Y, et al. Osteoimmunology: interplay between the immune system and bone metabolism. Annu Rev Immunol. 2006;24:33–63.

35. Kumar S, Boehm J, Lee JC. p38 MAP kinases: key signalling molecules as therapeutic targets for inflammatory diseases. Nat Rev Drug Discov. 2003;2(9):717–26.
36. Ashwell JD. The many paths to p38 mitogen-activated protein kinase activation in the immune system. Nat Rev Immunol. 2006; 6(7):532–40.
37. Fujita K, Iwasaki M, Ochi H, et al. Vitamin E decreases bone mass by stimulating osteoclast fusion. Nat Med. 2012;18(4):589–94.
38. Bohm C, Hayer S, Kilian A, et al. The alpha-isoform of p38 MAPK specifically regulates arthritic bone loss. J Immunol. 2009;183(9): 5938–47.
39. Tian B, Jiang T, Shao Z, et al. The prevention of titanium-particle-induced osteolysis by OA-14 through the suppression of the p38 signaling pathway and inhibition of osteoclastogenesis. Biomaterials. 2014;35(32):8937–50.
40. Jeong BC, Kim JH, Kim K, Kim I, Seong S, Kim N. ATF3 modulates calcium signaling in osteoclast differentiation and activity by associating with c-Fos and NFATc1 proteins. Bone. 2017;95: 33–40.
41. Sato K, Suematsu A, Nakashima T, et al. Regulation of osteoclast differentiation and function by the CaMK-CREB pathway. Nat Med. 2006;12(12):1410–6.
42. Ha J, Kim HJ, Huang H, Lee ZH, Kim HH. Mitogen- and stress-activated protein kinase 1 activates osteoclastogenesis in vitro and affects bone destruction in vivo. J Mol Med (Berl). 2013; 91(8):977–87.